

Low-Energy Excitation Spectra in the Excitonic Phase of Cobalt Oxides

Tomoki Yamaguchi^{1*}, Koudai Sugimoto², and Yukinori Ohta¹

¹*Department of Physics, Chiba University, Chiba 263-8522, Japan*

²*Center for Frontier Science, Chiba University, Chiba 263-8522, Japan*

We study the excitonic phase and low-energy excitation spectra of perovskite cobalt oxides. Constructing the five-orbital Hubbard model defined on the three-dimensional cubic lattice for the $3d$ bands of $\text{Pr}_{0.5}\text{Ca}_{0.5}\text{CoO}_3$, we calculate the excitonic susceptibility in the normal state in the random-phase approximation (RPA) to show the presence of the instability toward excitonic condensation. On the basis of the excitonic ground state with a magnetic multipole obtained in the mean-field approximation, we calculate the dynamical susceptibility of the excitonic phase in the RPA and find that there appear a gapless collective excitation in the spin-transverse mode (Goldstone mode) and a gapful collective excitation in the spin-longitudinal mode (Higgs mode). The experimental relevance of our results is discussed.

The Bose–Einstein condensation of fermion pairs is one of the most intriguing phenomena in condensed matter physics. The excitonic phase (EP) is representative of such a pair condensation,^{1–4)} where holes in valence bands and electrons in conduction bands spontaneously form pairs owing to attractive Coulomb interaction. After Mott’s prediction of the EP half a century ago,⁵⁾ a number of candidate materials for this phase have come to our attention. Among them are the transition-metal chalcogenides $1T\text{-TiSe}_2$ ^{6–8)} and Ta_2NiSe_5 ,^{9–11)} where the electrons and holes on different atoms are considered to form spin-singlet pairs to condense into the EP, which is accompanied by lattice distortion.¹²⁾

Another class of materials includes the perovskite cobalt oxides,^{13–15)} where the valence-band holes and conduction-band electrons form spin-triplet pairs in different orbitals on the same atoms. $\text{Pr}_{0.5}\text{Ca}_{0.5}\text{CoO}_3$ (PCCO) is an example in which the “metal-insulator” phase transition is observed at $T_c \simeq 80$ K, which is associated with a sharp peak in the temperature dependence of the specific heat and a drop in the magnetic susceptibility below T_c ,¹⁶⁾ together with a valence transition of Pr ions.^{17,18)} Some results of experiments indicate that the resistivity is in fact small and nearly temperature independent below T_c ,¹⁹⁾ suggesting that the bands may not be fully gapped. Note that no local magnetic moments are observed, but the exchange splitting of the Pr^{4+} Kramers doublet occurs,¹⁹⁾ the result of which may therefore be termed as a *hidden* order, and also that no clear signatures of the spin-state transition are observed in the X-ray absorption spectra.^{19,20)}

Kuneš and Augustinský argued that the anomalies of PCCO can be attributed to the EP transition,¹³⁾ whereby they applied the dynamical-mean-field-theory calculation to the two-orbital Hubbard model defined on

a two-dimensional square lattice and claimed that the anomalous behaviors of the specific heat, dc conductivity, and spin susceptibility can be explained. They also performed the LDA+ U band-structure calculation and showed that the magnetic multipole ordering occurs in PCCO as a result of the excitonic condensation. LaCoO_3 under a high magnetic field is another example of the possible realization of the EP,²¹⁾ which was substantiated by the theoretical calculations based on the two-orbital Hubbard and related models in two-dimension.^{22,23)} In these materials, cobalt ions are basically in the Co^{3+} valence state with a $3d^6$ configuration, where the three t_{2g} orbitals are mostly filled with electrons and the two e_g orbitals are nearly empty. The low-spin state is thus favorable for the condensation of excitons.

In this work, motivated by the above development in the field, we will study the EP of PCCO using a realistic Hubbard model, taking into account all five $3d$ orbitals of Co ions arranged in the three-dimensional cubic lattice of the perovskite structure. The noninteracting tight-binding bands are determined from first principles and the electron-electron interactions in the $3d$ orbitals are fully taken into account in each Co ion. We will then study the excitonic fluctuations in the normal state via the calculation of the excitonic susceptibility in the random phase approximation (RPA) and show that the instability toward the EP actually occurs in this model. The ground state of this model is then calculated in the mean-field approximation, whereby we find that the EP with a magnetic multipole order actually occurs. We will also calculate the dynamical susceptibility of both spin-transverse and spin-longitudinal modes in the EP to clarify the presence of the gapless Goldstone and gapful Higgs modes in the excitation spectra. The experimental relevance of our results will be discussed.

The crystal structure of PCCO belongs to the P_{nma}

*t.yamaguchi@chiba-u.jp

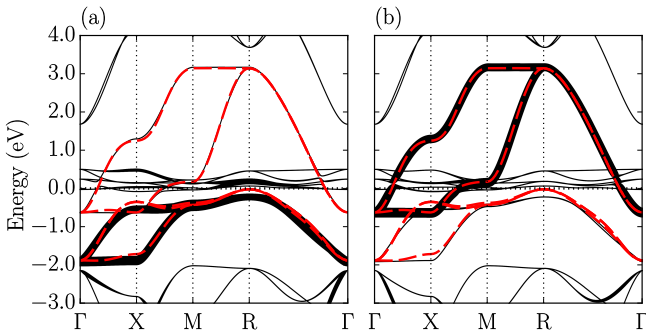


Fig. 1. (Color online) Calculated band dispersions of PrCoO₃ plotted along the lines connecting $\Gamma(0, 0, 0)$, $X(\pi, 0, 0)$, $M(\pi, \pi, 0)$, and $R(\pi, \pi, \pi)$. The width of the black solid curves is in proportion to the weight of (a) the Co t_{2g} orbitals and (b) the Co e_g orbitals. The tight-binding band dispersions obtained using the maximally localized Wannier functions are also shown by red dashed curves.

space group, where the CoO₆ octahedra are rotated and the cubic perovskite structure is distorted with two independent Co ions in the unit cell,¹⁶⁾ giving rise to complexity in the analysis of the EP in PCCO. We instead make use of the crystal structure of PrCoO₃, which is a perfect cubic perovskite with the lattice constant $a = 3.82 \text{ \AA}$ ²⁴⁾ (hereafter taken as the unit of length). The electronic structure is then calculated from first principles using the WIEN2k code.²⁵⁾ The obtained band dispersions are illustrated in Fig. 1, where we find that the bands near the Fermi energy come from the Pr $4f$ orbitals (giving narrow dispersions) and Co $3d$ orbitals (giving wide dispersions). For the latter, we find that the valence bands come from the t_{2g} manifold of Co $3d$ orbitals and the conduction bands come from the e_g manifold, as indicated in the weight plot. We, moreover, find that the t_{2g} bands and e_g bands are orthogonal to each other without hybridization, providing us with an ideal situation for excitonic condensation. We also performed the band-structure calculation of PCCO, arranging the Pr and Ca ions regularly, and confirmed that the bands remain qualitatively unchanged, supporting the validity of the rigid-band approximation. Note that PCCO contains both the Co³⁺ and Co⁴⁺ ions,¹⁹⁾ while PrCoO₃ contains only the Co³⁺ ions and shows no signatures of the phase transition.²⁶⁾ The change in the valence state of Co ions, which may lead to a better nesting feature of the Fermi surfaces, seems to play an important role in the EP transition. Hereafter, we focus on the $3d$ bands of the Co ions, and assuming that the $4f$ bands of Pr ions act as a bath of electrons and, together with the presence of Ca²⁺ ions, the valence state of Co ions is kept to be in the $3d^6$ configuration for simplicity¹³⁾ unless otherwise stated.

Let us now set up the Hamiltonian $H = H_0 + H_{\text{int}}$ for the modeling of the $3d$ electrons of PCCO. The kinetic energy term H_0 is defined in the tight-binding approxi-

mation as

$$H_0 = \sum_{i,\mu,\sigma} \epsilon_\mu c_{i,\mu,\sigma}^\dagger c_{j,\mu,\sigma} + \sum_{i,j} \sum_{\mu,\nu} \sum_{\sigma} t_{ij,\mu\nu} c_{i,\mu,\sigma}^\dagger c_{j,\nu,\sigma}, \quad (1)$$

where $c_{i,\mu,\sigma}^\dagger$ is the creation operator of a spin- σ ($=\uparrow, \downarrow$) electron on the orbital μ at site i , ϵ_μ is the on-site energy of orbital μ , and $t_{ij,\mu\nu}$ is the hopping integral between the orbital ν at site j and the orbital μ at site i . The orbitals μ and ν are labeled as 1 (d_{xy}), 2 (d_{yz}), 3 (d_{zx}), 4 ($d_{x^2-y^2}$), and 5 ($d_{3z^2-r^2}$). The 12 molecular orbitals for the $3d$ and $4f$ bands are obtained as the maximally localized Wannier functions,^{27,28)} thereby retaining only the $3d$ bands to determine the on-site energies and hopping integrals (up to 6th neighbors). The tight-binding band dispersions thus calculated reproduce the first-principles band structure well, as shown in Fig. 1.

The on-site interaction term is defined as

$$\begin{aligned} H_{\text{int}} = & \frac{U}{2} \sum_{i,\mu,\sigma} c_{i\mu\sigma}^\dagger c_{i\mu\sigma} c_{i\mu-\sigma}^\dagger c_{i\mu-\sigma} \\ & + \frac{U'}{2} \sum_{i,\sigma,\sigma'} \sum_{\mu \neq \nu} c_{i,\mu,\sigma}^\dagger c_{i,\mu,\sigma} c_{i,\nu,\sigma'}^\dagger c_{i,\nu,\sigma'} \\ & - \frac{J}{2} \sum_{i,\sigma,\sigma'} \sum_{\mu \neq \nu} c_{i,\mu,\sigma}^\dagger c_{i,\mu,\sigma'} c_{i,\nu,\sigma'}^\dagger c_{i,\nu,\sigma} \\ & + \frac{J'}{2} \sum_{i,\sigma} \sum_{\mu \neq \nu} c_{i,\mu,\sigma}^\dagger c_{i,\nu,-\sigma} c_{i,\nu,-\sigma}^\dagger c_{i,\mu,\sigma}, \end{aligned} \quad (2)$$

where U, U', J , and J' are the intraorbital Coulomb interaction, interorbital Coulomb interaction, Hund's rule coupling, and pair-hopping interaction, respectively. We assume the atomic-limit relations $U' = U - 2J$ and $J' = J$ for the interaction strengths, and we fix the ratio J/U at 0.1 in the present calculations.

We apply the mean-field approximation to the interaction terms. We assume the spin-triplet excitonic order in the presence of Hund's rule coupling²⁹⁾ and write the order parameters as

$$\Delta_{\mu,\nu} = \sum_{\mathbf{k},\sigma} \sigma \left\langle c_{\mathbf{k}+\mathbf{Q},\mu,\sigma}^\dagger c_{\mathbf{k},\nu,\sigma} \right\rangle, \quad (3)$$

where $c_{\mathbf{k},\mu,\sigma}$ is the Fourier component of $c_{i,\mu,\sigma}$ with the wave vector \mathbf{k} , and \mathbf{Q} is an ordering vector. Note that when μ (ν) is one of the e_g orbitals, ν (μ) is one of the t_{2g} orbitals. All the terms irrelevant to this excitonic ordering are neglected for simplicity. We thus obtain the diagonalized mean-field Hamiltonian,

$$H^{\text{MF}} = \sum_{\mathbf{k}_0,\epsilon,\sigma} E_{\mathbf{k}_0,\epsilon,\sigma} \gamma_{\mathbf{k}_0,\epsilon,\sigma}^\dagger \gamma_{\mathbf{k}_0,\epsilon,\sigma}, \quad (4)$$

where $\gamma_{\mathbf{k}_0,\epsilon,\sigma}$ is the canonical transformation of $c_{\mathbf{k},\mu,\sigma}$ satisfying $c_{\mathbf{k},\mu,\sigma} = \sum_{\epsilon} \psi_{\mu,m;\epsilon}(\mathbf{k}_0,\sigma) \gamma_{\mathbf{k}_0,\epsilon,\sigma}$ and ϵ is the band index. Since the excitonic order enlarges the unit cell, we write the wave vector as $\mathbf{k} = \mathbf{k}_0 + m\mathbf{Q}$, where \mathbf{k}_0

Table I. Nonzero elements of $V_{\mu\lambda}^{ss'}$, where $s = (\sigma_1, \sigma_2)$ and $s' = (\sigma'_1, \sigma'_2)$.

	$\sigma_1 = \sigma_2$ $= \sigma'_1 = \sigma'_2$	$\sigma_1 = \sigma_2$ $\neq \sigma'_1 = \sigma'_2$	$\sigma_1 = \sigma'_2$ $\neq \sigma_2 = \sigma'_1$
$\mu = \nu = \kappa = \lambda$	–	$-U$	U
$\mu = \kappa \neq \nu = \lambda$	–	$-J$	J
$\mu = \nu \neq \kappa = \lambda$	$-U + 3J$	$-U + 2J$	J
$\mu = \lambda \neq \nu = \kappa$	$U - 3J$	$-J$	$U - 2J$

is the wave vector in the reduced Brillouin zone and m is an integer. We carry out the summation with respect to \mathbf{k}_0 using the $50 \times 50 \times 50$ meshes in the reduced Brillouin zone.

We define the dynamical susceptibility as

$$\chi_{\lambda\mu}^{ss'}(\mathbf{q}, \mathbf{q}', \omega) = \frac{i}{N} \sum_{\mathbf{k}, \mathbf{k}'} \int_0^\infty dt e^{i\omega t} \times \langle [c_{\mathbf{k}, \kappa, \sigma_1}^\dagger(t) c_{\mathbf{k}+\mathbf{q}, \lambda, \sigma_2}(t), c_{\mathbf{k}'+\mathbf{q}', \mu, \sigma'_1}^\dagger c_{\mathbf{k}', \nu, \sigma'_2}] \rangle, \quad (5)$$

where N is the number of \mathbf{k} points used, $c_{\mathbf{k}, \mu, \sigma}(t)$ is the Heisenberg representation of $c_{\mathbf{k}, \mu, \sigma}$, and s denotes a spin pair (σ_1, σ_2) , taking the values $\uparrow, \downarrow, +$, and $-$ for $(\uparrow, \uparrow), (\downarrow, \downarrow), (\uparrow, \downarrow)$, and (\downarrow, \uparrow) , respectively. We write Eq. (5) as $\chi(\mathbf{q}, \omega)$ when $\mathbf{q} = \mathbf{q}'$. The bare susceptibility is given by

$$\begin{aligned} & \chi_0^{ss'}{}_{\lambda\mu}(\mathbf{q}, \mathbf{q} + l\mathbf{Q}, \omega) \\ &= -\frac{1}{N} \sum_{\mathbf{p}_0, m, n, \epsilon, \epsilon'} \frac{f(E_{\mathbf{p}_0+\mathbf{q}, \epsilon, \sigma_1}) - f(E_{\mathbf{p}_0, \epsilon', \sigma_2})}{E_{\mathbf{p}_0+\mathbf{q}, \epsilon, \sigma_1} - E_{\mathbf{p}_0, \epsilon', \sigma_2} - (\omega + i\eta)} \\ & \times \psi_{\lambda, m; \epsilon}(\mathbf{p}_0 + \mathbf{q}, \sigma_1) \psi_{\mu, m+n+l; \epsilon}^*(\mathbf{p}_0 + \mathbf{q}, \sigma'_2) \\ & \times \psi_{\kappa, m; \epsilon'}^*(\mathbf{p}_0, \sigma_2) \psi_{\nu, m+n; \epsilon'}(\mathbf{p}_0, \sigma'_1) \delta_{\sigma_1, \sigma'_2} \delta_{\sigma'_1, \sigma_2}, \quad (6) \end{aligned}$$

where the summation with respect to \mathbf{p}_0 runs over the reduced Brillouin zone. We set $\eta = 0.01$ eV.

We calculate the dynamical susceptibilities in the multiorbital RPA, given by

$$\begin{pmatrix} \chi^{+-} \\ \chi^{\uparrow\uparrow} \\ \chi^{\downarrow\downarrow} \end{pmatrix} = \begin{pmatrix} \chi_0^{+-} \\ \chi_0^{\uparrow\uparrow} \\ 0 \end{pmatrix} + \begin{pmatrix} \chi_0^{+-} V^{-+-} & 0 & 0 \\ 0 & \chi_0^{\uparrow\uparrow} V^{\uparrow\uparrow} & \chi_0^{\uparrow\uparrow} V^{\uparrow\downarrow} \\ 0 & \chi_0^{\downarrow\downarrow} V^{\downarrow\uparrow} & \chi_0^{\downarrow\downarrow} V^{\downarrow\downarrow} \end{pmatrix} \begin{pmatrix} \chi^{+-} \\ \chi^{\uparrow\uparrow} \\ \chi^{\downarrow\downarrow} \end{pmatrix}, \quad (7)$$

where the matrix product in the orbital basis is given as

$$[\chi_0 V \chi]_{\lambda\mu}(\mathbf{q}, \omega) = \sum_{\kappa', \lambda', \mu', \nu', m} \chi_{0, \lambda\mu'}(\mathbf{q}, \mathbf{q} + m\mathbf{Q}, \omega) V_{\mu'\lambda'} V_{\nu'\kappa'} \chi_{\kappa'\nu'}(\mathbf{q} + m\mathbf{Q}, \omega) \quad (8)$$

with the interaction matrix V listed in Table I.

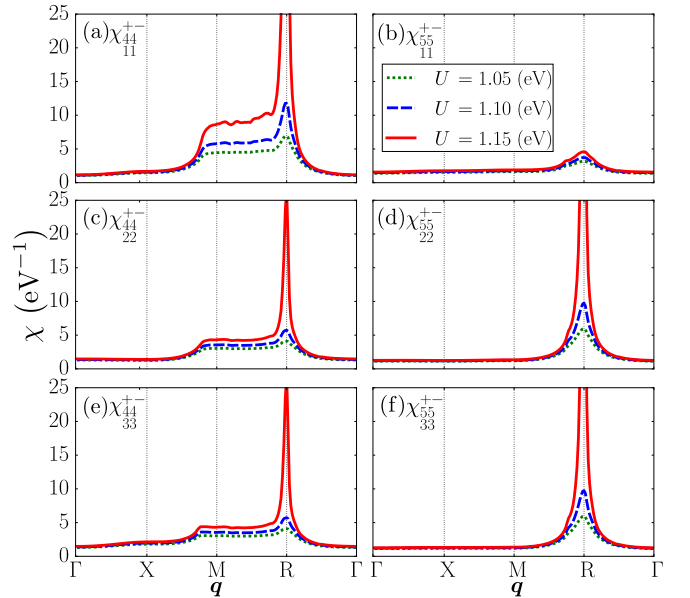


Fig. 2. (Color online) Calculated static susceptibility $\chi_{\mu\nu}^{+-}$ in the normal phase. The red-solid, blue-dashed, and green-dotted lines are for $U = 1.15, 1.1$, and 1.05 eV, respectively.

First, let us discuss the spin-triplet excitonic fluctuations in the normal phase. Figure 2 shows the \mathbf{q} dependence of the static susceptibility of the excitonic spin-transverse mode $\chi_{\mu\nu}^{+-}(\mathbf{q}, \omega = 0)$ calculated in the normal phase, where μ (ν) is one of the e_g (t_{2g}) orbitals. We find that, at $\mathbf{q} = (\pi, \pi, \pi)$, the diverging fluctuations with increasing U toward 1.15 eV are observed for all the orbital components except $(\mu, \nu) = (5, 1)$. This instability toward the EP is caused by the Fermi-surface nesting between the electron pockets of the e_g bands located around the Γ point of the Brillouin zone and the hole pockets of the t_{2g} bands located around the $R(\pi, \pi, \pi)$ point of the Brillouin zone (see Fig. 1). Thus, the EP transition with the ordering vector $\mathbf{Q} = (\pi, \pi, \pi)$ occurs at the critical value $U_{\text{cr}} = 1.15$ eV.

Next, let us solve the mean-field equations to calculate the excitonic order parameter with $\mathbf{Q} = (\pi, \pi, \pi)$. The obtained orbital components $\Delta_{\mu, \nu}$ are shown in Fig. 3(a), where we find that all the components $\Delta_{\mu, \nu}$ (except $\Delta_{1,5}$) become finite above $U_{\text{cr}} = 1.15$ eV. As U increases, U' and J also increase, which enhances $\Delta_{\mu, \nu}$. Because the excitons are formed in a single atom, the excitonic spin polarization leads to the magnetic multipole order in real space,^{13,30} as shown in Fig. 3(b). The orbital components of the magnetic multipoles formed between the μ and ν orbitals (indicated as $\mu \otimes \nu$) are shown in Fig. 3(c). Reflecting the symmetry of the orbitals, the components of the order parameter satisfy the relations $\Delta_{4,2} = \Delta_{4,3} = \Delta_{4,1}/\sqrt{3}$, $\Delta_{5,2} = -\Delta_{5,3} = \Delta_{4,1}/2$, and $\Delta_{5,1} = 0$, where different combinations of the signs are also possible. The last relation indicates that the elec-

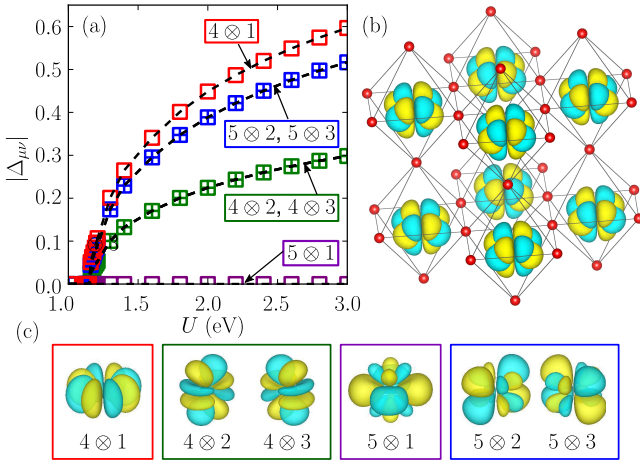


Fig. 3. (Color online) (a) Calculated U -dependence of excitonic order parameters $\Delta_{\mu,\nu}$. (b) Calculated magnetic multipole ordering corresponding to the excitonic order parameter at $U = 2.5$ eV. (c) Schematic representations of the orbital components of the magnetic multipoles.

trons on the $d_{3z^2-r^2}$ orbital and holes on the d_{xy} orbital do not form pairs. This is consistent with the result for the calculated excitonic susceptibility in the normal phase [see Fig. 2(b)], where no diverging behavior is observed. We note that the bands in the EP are not fully gapped at $U < 1.8$ eV, keeping the system metallic with small Fermi surfaces, which may be consistent with the results of experiment.¹⁹⁾ A full gap opens for larger values of $U > 1.8$ eV. We also note that the excitonic order remains finite against the change in the filling of electrons, e.g., between 5.4 and 6.1 per site at $U = 1.2$ eV, which is also consistent with experimental results.¹⁹⁾

Next, let us discuss the excitation spectra in the EP. The calculated excitonic spin-transverse dynamical susceptibilities $\text{Im} \chi_{\mu\nu}^{+-}$ are shown in Figs. 4(a)–4(d), where we find the gapless Goldstone mode at $\mathbf{q} = (\pi, \pi, \pi)$ for all the components except for $(\mu, \nu) = (5, 1)$ [see Fig. 4(c)], reflecting the presence/absence of $\Delta_{\mu,\nu}$. The velocities of the collective excitations near $\mathbf{q} = (\pi, \pi, \pi)$ are the same for all the components. Unlike in the well-known collective mode of the Heisenberg antiferromagnets, the excitonic collective mode does not extend to reach the point $\mathbf{q} = 0$ and $\omega = 0$. The gapless collective-mode behavior obtained is consistent with the results of the two-orbital models.^{14, 31)} Note that the excitations around $\mathbf{q} = (\pi/2, \pi/2, \pi/2)$ appearing in all the components originate from the particle-hole excitations. The calculated excitonic spin-longitudinal dynamical susceptibilities $\text{Im} \chi_{\mu\nu}^{zz}$ defined as $\chi_{\mu\nu}^{zz} = \sum_{\sigma, \sigma'} \sigma \sigma' \chi_{\lambda\mu}^{\sigma\sigma'}$ are also shown in Figs. 4(f)–4(i), where we find the gapful Higgs mode. The broad excitations that have a gap at $\mathbf{q} = (\pi, \pi, \pi)$ are clearly seen, except for $(\mu, \nu) = (5, 1)$ [see Fig. 4(h)], where only the particle-hole excitations

are present. The spectra around $\mathbf{q} = (\pi/2, \pi/2, \pi/2)$ appearing in all the components are again particle-hole excitations. The orbital-diagonal part of the dynamical susceptibilities in the transverse mode, $\sum_{\mu,\nu} \text{Im} \chi_{\mu\nu}^{+-}$, and in the longitudinal mode, $\sum_{\mu,\nu} \text{Im} \chi_{\mu\nu}^{zz}$, are also shown for comparison in Figs. 4(e) and 4(j), respectively, the results of which reflect the metallic nature of the system.

Finally, let us discuss the possible experimental relevance of our results. Inelastic neutron scattering may be a possible experimental technique for observing the excitations in the spin degrees of freedom, but may enable one to detect only the orbital-diagonal components of the dynamical susceptibility, the intensity of which is in proportion to $\sum_{\mu,\nu} \text{Im} \chi_{\mu\nu}^{ss'}$. Our corresponding results, which come from the particle-hole transitions, are shown in Figs. 4(e) and 4(j). Because the dynamical susceptibility related to the orbital-off-diagonal excitonic ordering should contain the vertex-nonconserved terms, defined as the terms with $\kappa \neq \lambda$ and $\mu \neq \nu$ in Eq. (5), we need to seek other quantum-beam sources that have the ability to change the orbitals (or orbital angular momentum) in the inelastic scattering processes. To this end, future experimental developments are desired.

In summary, we derived the effective five-orbital Hubbard model defined on the three-dimensional cubic lattice from first principles to describe the electronic states of $\text{Pr}_{0.5}\text{Ca}_{0.5}\text{CoO}_3$ with the cubic perovskite structure. Then, we calculated the static susceptibility of the excitonic spin-transverse mode in the normal phase using the RPA and found that the diverging excitonic fluctuations occur at $\mathbf{Q} = (\pi, \pi, \pi)$. We calculated the excitonic ground state in the mean-field approximation and found that the magnetic multipole order occurs. We also calculated the dynamical susceptibility in the EP to study the excitation spectra and found that there appear gapless collective excitations in the excitonic spin-transverse mode and gapful collective excitations in the excitonic spin-longitudinal mode.

Acknowledgment We thank T. Kaneko and S. Miyakoshi for fruitful discussions. This work was supported in part by Grants-in-Aid for Scientific Research from the Japan Society for the Promotion of Science (Nos. 26400349 and 15H06093). The numerical calculations were carried out on computers at Yukawa Institute for Theoretical Physics, Kyoto University, Japan, and Research Center for Computational Science, Okazaki, Japan.

- 1) D. Jérôme, T. M. Rice, and W. Kohn, Phys. Rev. **158**, 462 (1967).
- 2) B. I. Halperin and T. M. Rice, Rev. Mod. Phys. **40**, 755 (1968).
- 3) P. B. Littlewood, P. R. Eastham, J. M. J. Keeling, F. M. Marchetti, B. D. Simons, and M. H. Szymanska, J. Phys.: Condens. Matter **16**, S3597 (2004).
- 4) J. Kuneš, J. Phys.: Condens. Matter **27**, 333201 (2015).
- 5) N. F. Mott, Philos. Mag. **6**, 287 (1961).

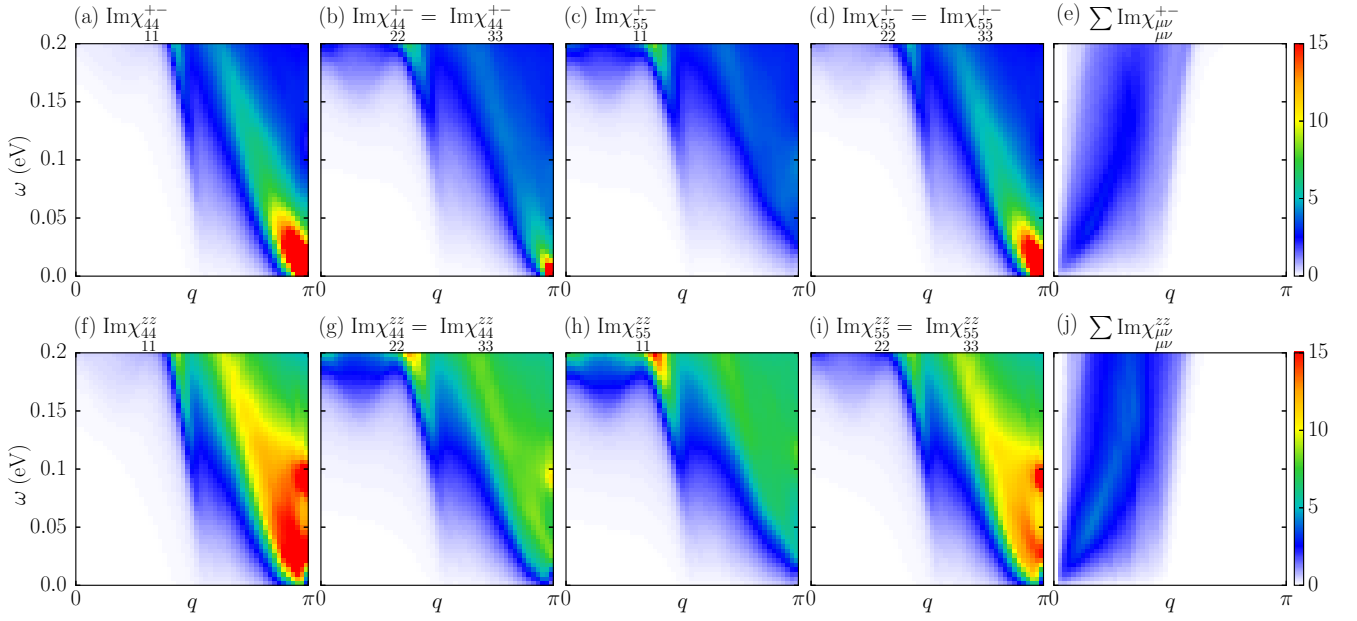


Fig. 4. (Color online) Calculated excitonic spin-transverse (upper panels) and spin-longitudinal (lower panels) modes of the dynamical susceptibility in the EP. The orbital-diagonal part of the dynamical susceptibility in (e) the spin-transverse and (j) spin-longitudinal modes is also shown. The path of the wave vector is along the line from $\mathbf{q} = (0, 0, 0)$ to (π, π, π) . The interaction strength is assumed to be $U = 1.2$ eV.

- 6) F. J. Di Salvo, D. E. Moncton, and J. V. Waszczak, *Phys. Rev. B* **14**, 4321 (1976).
- 7) H. Cercellier, C. Monney, F. Clerc, C. Battaglia, L. Despont, M. G. Garnier, H. Beck, P. Aebi, L. Patthey, H. Berger, and L. Forró, *Phys. Rev. Lett.* **99**, 146403 (2007).
- 8) C. Monney, H. Cercellier, F. Clerc, C. Battaglia, E. F. Schwier, C. Didiot, M. G. Garnier, H. Beck, P. Aebi, H. Berger, L. Forró, and L. Patthey, *Phys. Rev. B* **79**, 45116 (2009).
- 9) Y. Wakisaka, T. Sudayama, K. Takubo, T. Mizokawa, M. Arita, H. Namatame, M. Taniguchi, N. Katayama, M. Nohara, and H. Takagi, *Phys. Rev. Lett.* **103**, 26402 (2009).
- 10) T. Kaneko, T. Toriyama, T. Konishi, and Y. Ohta, *Phys. Rev. B* **87**, 35121 (2013).
- 11) K. Seki, Y. Wakisaka, T. Kaneko, T. Toriyama, T. Konishi, T. Sudayama, N. L. Saini, M. Arita, H. Namatame, M. Taniguchi, N. Katayama, M. Nohara, H. Takagi, T. Mizokawa, and Y. Ohta, *Phys. Rev. B* **90**, 155116 (2014).
- 12) T. Kaneko, B. Zenker, H. Fehske, and Y. Ohta, *Phys. Rev. B* **92**, 115106 (2015).
- 13) J. Kuneš and P. Augustinský, *Phys. Rev. B* **90**, 235112 (2014).
- 14) J. Nasu, T. Watanabe, M. Naka, and S. Ishihara, *Phys. Rev. B* **93**, 205136 (2016).
- 15) J. F. Afonso and J. Kuneš, arXiv:1612.07576.
- 16) S. Tsubouchi, T. Kyōmen, M. Itoh, P. Ganguly, M. Oguni, Y. Shimojo, Y. Morii, and Y. Ishii, *Phys. Rev. B* **66**, 52418 (2002).
- 17) J. Hejtmánek, E. Šantavá, K. Knížek, M. Maryško, Z. Jirák, T. Naito, H. Sakaki, and H. Fujishiro, *Phys. Rev. B* **82**, 165107 (2010).
- 18) J. L. García-Muñoz, C. Frontera, A. J. Barón-González, S. Valencia, J. Blasco, R. Feyerherm, E. Dudzik, R. Abrudan, and F. Radu, *Phys. Rev. B* **84**, 045104 (2011).
- 19) J. Hejtmánek, Z. Jirák, O. Kaman, K. Knížek, E. Šantavá, K. Nitta, T. Naito, and H. Fujishiro, *Eur. Phys. J. B* **86**, 305 (2013).
- 20) J. Herrero-Martín, J. L. García-Muñoz, K. Kvashnina, E. Gallo, G. Subías, J. A. Alonso, and A. J. Barón-González, *Phys. Rev. B* **86**, 125106 (2012).
- 21) A. Ikeda, T. Nomura, S. Takeyama, Y. H. Matsuda, A. Matsuo, K. Kindo, and K. Sato, *Phys. Rev. B* **93**, 220401(R) (2016).
- 22) A. Sotnikov and J. Kuneš, *Sci. Rep.* **6**, 30510 (2016).
- 23) T. Tatsuno, E. Mizoguchi, J. Nasu, M. Naka, and S. Ishihara, *J. Phys. Soc. Jpn.* **85**, 083706 (2016).
- 24) W. Wei-Ran, X. Da-Peng, S. Wen-Hui, D. Zhan-Hui, X. Yan-Feng, and S. Geng-Xin, *Chin. Phys. Lett.* **22**, 2400 (2005).
- 25) P. Blaha, K. Schwarz, G. K. H. Madsen, D. Kvasnicka, and J. Luitz, WIEN2K (Technische Universität Wien, Austria, 2002).
- 26) S. K. Pandey, S. Patil, V. R. R. Medicherla, R. S. Singh, and K. Maiti, *Phys. Rev. B* **77**, 115137 (2008).
- 27) J. Kuneš, R. Arita, P. Wissgott, A. Toschie, H. Ikeda, and K. Helde, *Comput. Phys. Commun.* **181**, 1888 (2010).
- 28) A. A. Mostofi, J. R. Yates, G. Pizzi, Y. S. Lee, I. Souza, D. Vanderbilt, and N. Marzari, *Comput. Phys. Commun.* **185**, 2309 (2014).
- 29) T. Kaneko and Y. Ohta, *Phys. Rev. B* **90**, 245144 (2014).
- 30) T. Kaneko and Y. Ohta, *Phys. Rev. B* **94**, 125127 (2016).
- 31) P. M. R. Brydon and C. Timm, *Phys. Rev. B* **80**, 174401 (2009).